

We are IntechOpen, the world's leading publisher of Open Access books Built by scientists, for scientists

4,800

Open access books available

122,000

International authors and editors

135M

Downloads

Our authors are among the

154

Countries delivered to

TOP 1%

most cited scientists

12.2%

Contributors from top 500 universities



WEB OF SCIENCE™

Selection of our books indexed in the Book Citation Index
in Web of Science™ Core Collection (BKCI)

Interested in publishing with us?
Contact book.department@intechopen.com

Numbers displayed above are based on latest data collected.

For more information visit www.intechopen.com



Measurements and Characterization of Ultra Wideband Propagation within Spacecrafts- Proposal of Wireless Transmission for Replacing Wired Interface Buses

Akihisa Matsubara^{1,2}, Atsushi Tomiki²,
Tomoaki Toda² and Takehiko Kobayashi¹

¹*Tokyo Denki University,*

²*Japan Aerospace Exploration Agency,
Japan*

1. Introduction

This chapter describes measurement and characterization of radio propagation—particularly of ultra wideband (UWB) signals— within spacecrafts with a view to (at least partly) replacing onboard data buses with wireless connections. On-board equipment within spacecraft is classified into bus and mission parts. Bus parts are basic subsystems dealing with maintenance of the spacecraft system, such as Communication and Data Handling Subsystem, Attitude and Orbit Control Subsystem, Electrical Power Subsystem, Solar Array Paddle Subsystem, Temperature Control Subsystem, and Reaction Control Subsystem. Mission parts are important spacecraft subsystems vital to a mission's success, such as Scientific Instruments, Transponders, and Mission Data Processing Subsystems. Recently, due to more sophisticated spacecraft missions, mission parts have taken priority over bus parts in spacecraft design. As on-board submission equipment diversifies, wire harness used to connect subsystem components increase the weight of spacecraft. For example, about 4% (more than 20 kg) of the 500 kg of weight of Japan's Venus Climate Orbiter "AKATSUKI/Planet-C" spacecraft, launched in 2010, is signal wire-harness mass. Spacecraft manufacturing is largely a manual operation, with high costs and long lead times. Harnessing or electrical interconnections form a large part of spacecraft, contributing mass and requiring more assembly, integration, and testing as spacecraft complexity increases. Although wireless technologies have not been utilized within spacecraft as a physical layer of data buses, applying wireless technologies to a portion of signal wires could be extremely useful. Adoption of wireless technologies within spacecrafts could contribute to the following:

- Reduction of cable weight and resulting launching costs
- More flexibility in layout of spacecraft subsystems
- More reliable connections at rotary, moving, and sliding joints

To realize these benefits, multipath propagation affecting digital transmission performance must be scrutinized. Narrowband wireless communication systems, such as conventional wireless local area networks, deteriorate due to frequency-selective fading in multipath

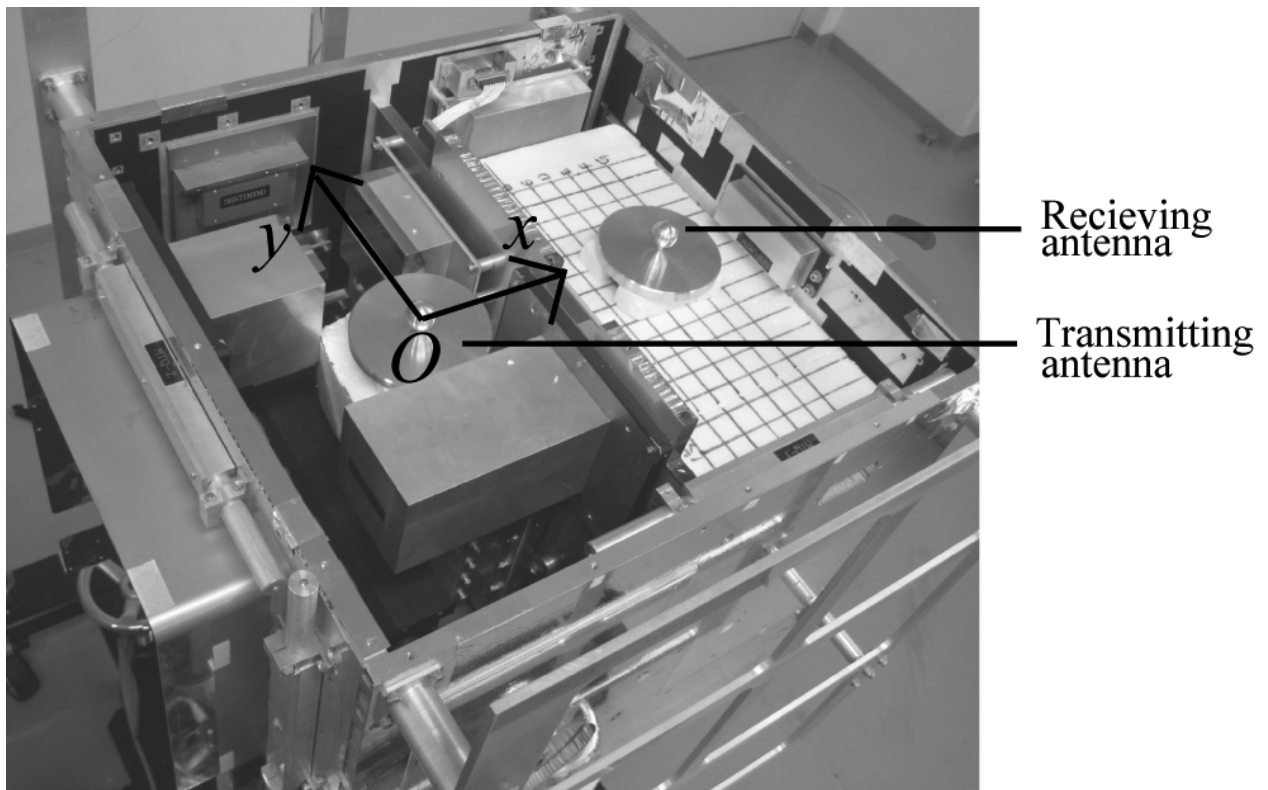
environments and hence need a substantial amount of fading margin (Kobayashi, 2006). In addition, intense long-delayed multipaths could cause inter symbol interference (ISI) and thus limit the data rate. Since UWB signals typically occupy a bandwidth of more than 500 MHz or a fractional bandwidth of more than 20%, they are expected to suffer less from multipath fading (Ghavami et al., 2007). While propagation of the UWB signals have been intensively measured and modeled in indoor and confined environments (Kobayashi, 2006; Win & Scholtz, 2002; Foerster, 2002; Haneda et al., 2006; Suzuki & Kobayashi, 2005; Gelabert et al., 2009), there has been only our study for spacecrafts. The study presented in this chapter proposes the use of UWB technology to facilitate a high data rate (e.g. maximum of 212 Mb/s per node attained with SpaceWire (European Cooperation for Space Standardization, 2003), equalling the standards of a wired onboard data bus) and to reduce fading margin.

The goal of this chapter is to measure and characterize radio propagation within a spacecraft and control it with the use of a radio absorber. In this study, UWB signal propagation (from 3.1 GHz to 10.6 GHz) in the frequency domain was measured and characterized with use of a microwave vector network analyzer. Spatial distributions of UWB and narrowband propagation gain, delay profiles (channel responses in the time domain), delay spreads (the second centered moments of the delay profiles), and the relation between fading depth and the bandwidth were derived from measurements conducted in a mechanical test model of a scientific satellite and a simulated shield box. Suppression of the delay spreads was attempted and evaluated by partially panelling a radio absorber on the inner surfaces.

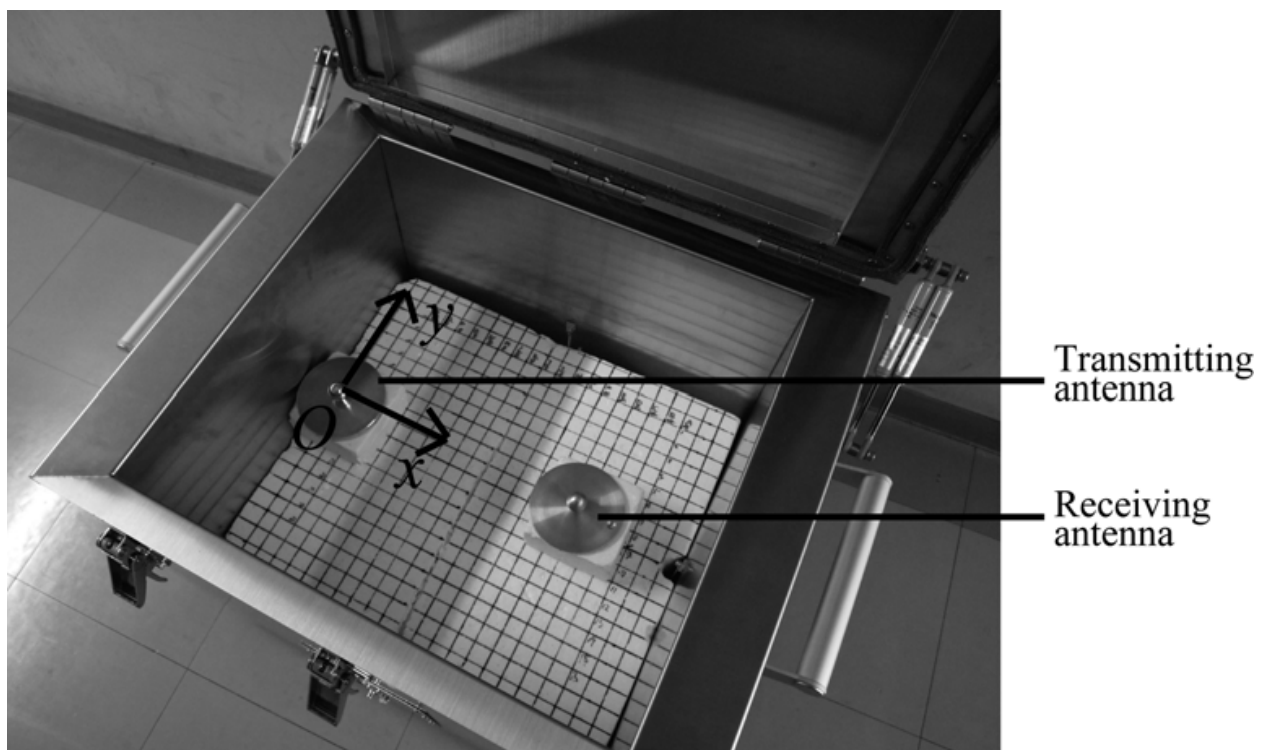
2. Measurement setup

A mechanical test model (MTM) of a small scientific satellite, which was launched in 2005, and a shield box of the same size were used for this measurement, as shown in Fig. 1. The MTM was a rectangular parallelepiped, 430 mm long \times 470 mm wide \times 435 mm high, enclosed in flat honeycomb panels made of aluminium, excluding its solar panels. Its interior was divided into two almost equal subspaces by a conductive partition having many openings, and mostly filled with mission subsystems. Hence, spatial distribution of the propagation gain would be attained only in a limited region. The shield box was employed to assess the whole inner space.

The transmitting and receiving antennas were omnidirectional, vertically polarized, low voltage-standing-wave-ratio UWB volcano-smoke antennas (Taniguchi et al., 2006), as shown in Fig. 2. Their circular ground planes were 100 mm in diameter. Within the MTM, the transmitting antenna was fixed in one subspace and the receiving antenna was scanned in another. During the measurements, the top lid was closed and the monopole elements of the two antennas were 3 mm below the lid. The x and y axes of the coordinate were parallel to the sides of the MTM, and the origin was located at the electric center of the transmitting antenna, as shown in Fig. 1(a). The receiving antenna was scanned within a region $200 \leq x$ [mm] ≤ 300 and $-140 \leq y$ [mm] ≤ 140 in 20-mm intervals on a styrofoam stage (transparent to electromagnetic waves). The feeding coaxial cables penetrated through the observation windows on the sides. Within the empty shield box, the transmitting antenna was fixed at 250 mm above the bottom and adjacent to the center of the 430-mm side, as shown in Fig. 1(b). That position was the origin of the coordinate, whose x and y axes were parallel to the sides. The receiving antenna was scanned horizontally within $0 \leq x$ [mm] ≤ 480 and $-180 \leq y$ [mm] ≤ 180 (excluding the close vicinity of the transmitting antenna) in 20-mm intervals on a styrofoam stage. During the measurements the conductive top lid was also closed. The feeding cables were relayed by coaxial connectors penetrating the wall.



(a)



(b)

Fig. 1. The measurement setup in: (a) a mechanical test model of small scientific satellite and (b) an empty shield box.



Fig. 2. Omnidirectional, low-VSWR UWB monopole antenna.

Frequency- (from 3.1 to 10.6 GHz) and time-domain propagation gains were measured with a microwave vector network analyzer. From the frequency-domain power gain data, the UWB propagation gains were calculated by integrating the power of the gains between the feeding points of the antennas over the occupied bandwidth:

$$PG_{\text{UWB}} = 10 \log \left(\frac{1}{f_H - f_L} \int_{f_L}^{f_H} 10^{\frac{PG_{\text{dB}}(f)}{10}} df \right) \quad (1)$$

where $PG_{\text{dB}}(f)$ is the propagation gain in dB measured at a frequency f , and f_L and f_H are the lowest and the highest frequencies, from 3.1 to 10.6 GHz (the full band approved in the United States) and from 7.3 to 7.9 GHz (the high band approved in Japan); and the continuous wave (CW) gain at the center frequency (= 6.85 GHz) was extracted therefrom. From the time-domain power gain data (power delay profile), the root-mean-square (rms) delay spread is the square root of the second central moment of a power delay profile. The delay spread is used to describe the average power delay profiles $P(\tau_i)$, where τ_i is the i th path delay. Average delay (D) and delay spread (S) are yielded by

$$D = \frac{\sum_{i=0}^n \tau_i P(\tau_i)}{\sum_{i=0}^n P(\tau_i)} \quad (2)$$

and

$$S = \frac{\sum_{i=0}^n (\tau_i - D)^2 P(\tau_i)}{\sum_{i=0}^n P(\tau_i)} \quad (3)$$

Delay spread estimates are sensitive to noise components having large excess delays. The usual way to cancel the effect of noise is by setting to zero the values of the power-delay profile lying below a noise threshold defined relative to the peak power in the profile. In this study, a threshold level in -20 dB below the maximum return was defined.

3. Measurement results

Examples of time- and frequency-domain propagation gains are presented in Figs. 3 and 4, measured at $(x, y) = (300, 0)$ within the MTM and the shield box. The delay spreads were computed at less than 20 ns for the MTM, and more than 100 ns for the shield box. In the frequency domain (Fig. 4), frequency selective fading occurs intensely within the MTM and the shield box. The spatial distributions of CW and UWB propagation gains within the MTM are shown in Fig. 5. Propagation gains ranged from -48 to -20 dB for CW (= 6.85 GHz), from -28 dB to -24 dB for the full UWB, from -28 to -21 dB for the low-band UWB, and from -30 dB to -26 dB for the high-band UWB in the MTM. Similar results were obtained within the shield box, as shown in Fig. 6. Propagation gains ranged from -41 to -6.1 dB for CW, from -15 to -12 dB for the full UWB, from -14 to -9.7 dB for the low-band UWB, and from -19 to -13 dB for the high-band UWB. The lower gains in the MTM than in the shield box were attributed to the non line-of-sight propagation paths intercepted by the conductive partition dividing the interior. The UWB propagation gains did not exhibit explicit dependence on distance, whereas the IEEE 802.15.3a (Foerster, 2002) channel model applicable to indoor environments used the path loss increasing with the square of distance. While CW resulted in up to 28 dB (in the MTM) and 35 dB (in the shield box) fading at several “dead spots” caused by multipath interference, UWB practically yielded no dead spots. The fading depth versus frequency bandwidth at the deepest dead spots $(x, y) = (300, 60)$ in the MTM and $(180, -60)$ in the shield box were derived from measured data, as shown in Fig. 7, where the center frequency was fixed at 6.85 GHz, and the 7.5-GHz-bandwidth (from 3.1 to 10.6 GHz) propagation gain was set to the 0-dB reference. A bandwidth over 400 MHz or a fractional bandwidth over 6% was capable of reducing the fading depth to approximately 2 dB for both the MTM and the shield box.

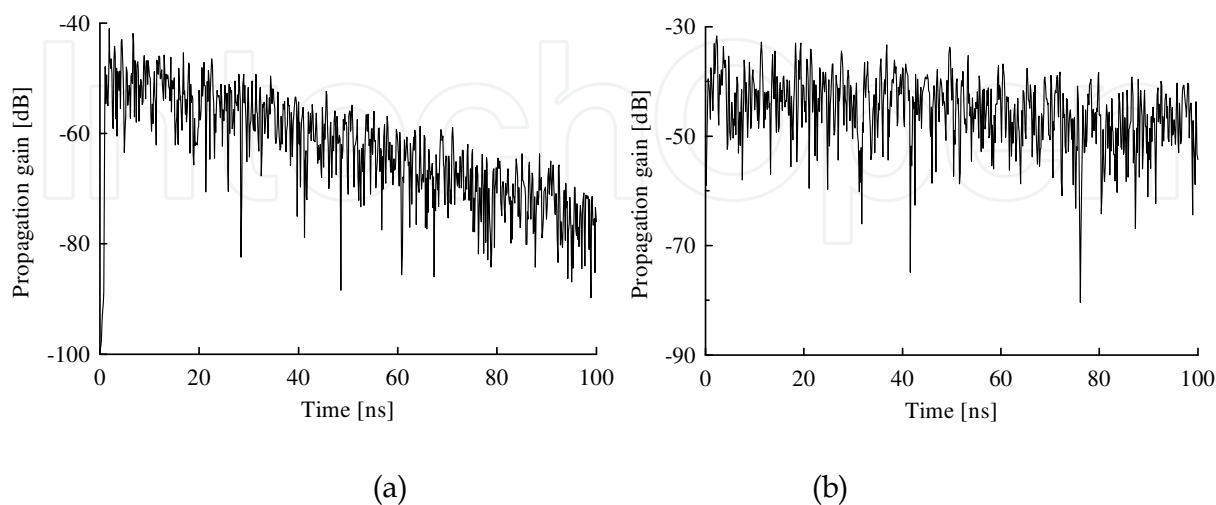


Fig. 3. Delay profiles at $(300, 0)$ in (a) the MTM and (b) the shield box.

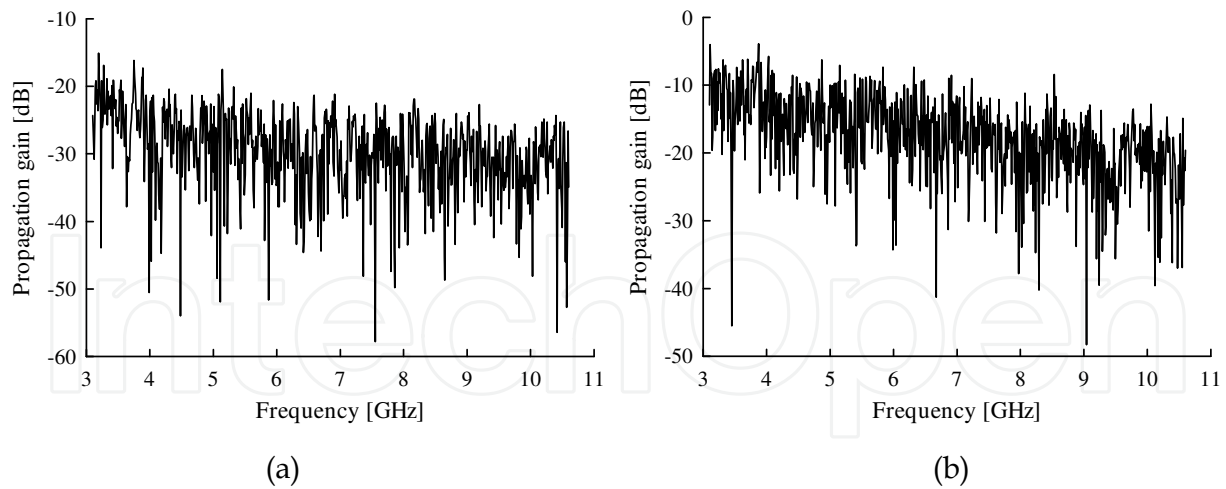


Fig. 4. Frequency responses at (300, 0) in (a) the MTM and (b) the shield box.

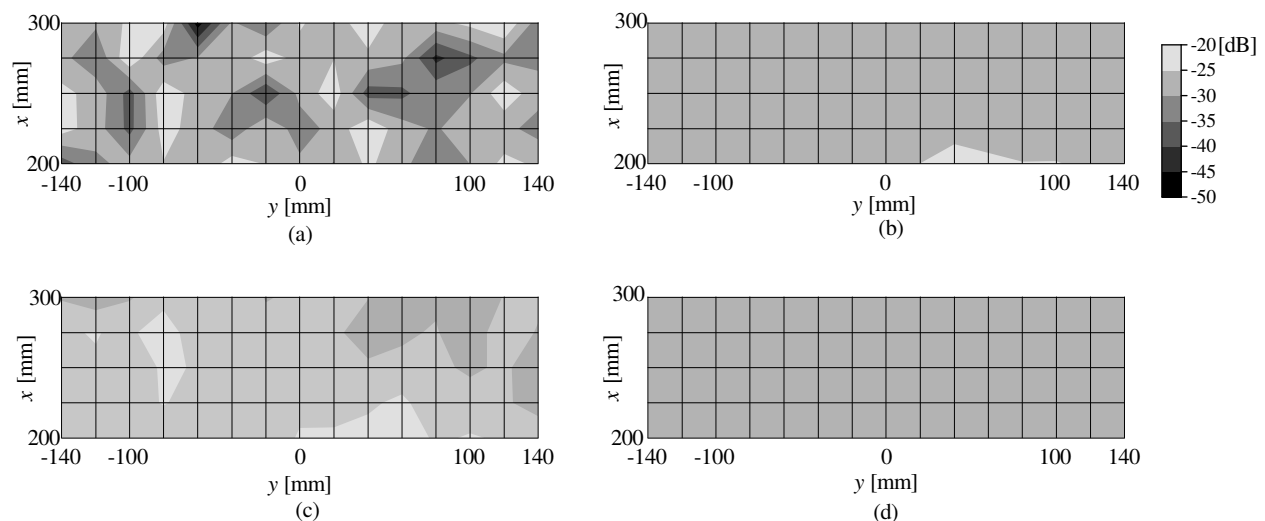


Fig. 5. Spatial distributions of propagation gain within the MTM: (a) CW (6.85 GHz), (b) fullband UWB (3.1 - 10.6 GHz), (d) low-band UWB (4.2 - 4.8 GHz), and (c) high-band UWB (7.3 - 7.9 GHz).

4. Suppression of delay spreads

The conductive enclosures yields a long delay spread, particularly when empty, which causes inter symbol interference (ISI), and hence an irreducible error floor when the modulation symbol time is on the same order as the delay spread. A patch of a thin elastic radio absorber, shown in Fig. 8, was attached at the center of the bottom of the shield box to suppress the delay spreads. The absorbers, 2.3 and 1.8 mm thick, usable in vacuum, attenuated radio wave reflection by 20 dB at 4 and 7 GHz, respectively, and by 10 dB within a 1.5-GHz bandwidth. Propagation properties were measured while the patch of the strip was $0.093 \text{ m}^2 (= 305 \text{ mm square}) \times 2^{-n}$, where $n = 0, 1, 2, \dots, 6$, corresponding $8 \times 2^{-n}\%$ against the total inner surface. Examples of delay profiles are shown in Fig. 9, when the receiving antenna was placed at $(x, y) = (300, 0)$. The conductive empty shield box caused abundant multipaths. The long delays were suppressed with use of the radio absorber. Relation

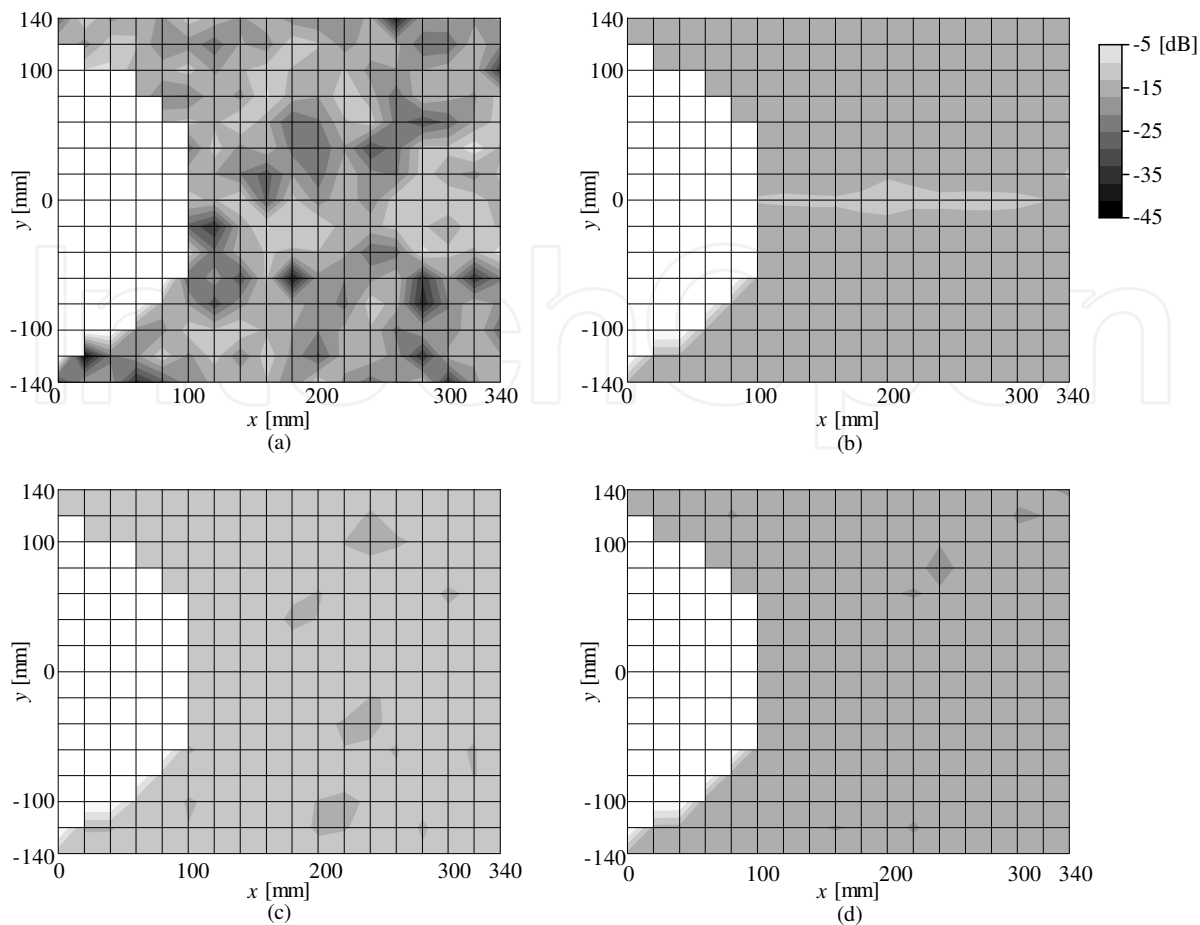


Fig. 6. Spatial distributions of propagation gain within the shield box: (a) CW (6.85 GHz), (b) full-band UWB (3.1 - 10.6 GHz), (d) low-band UWB (4.2 - 4.8 GHz), and (c) high-band UWB (7.3 - 7.9 GHz).

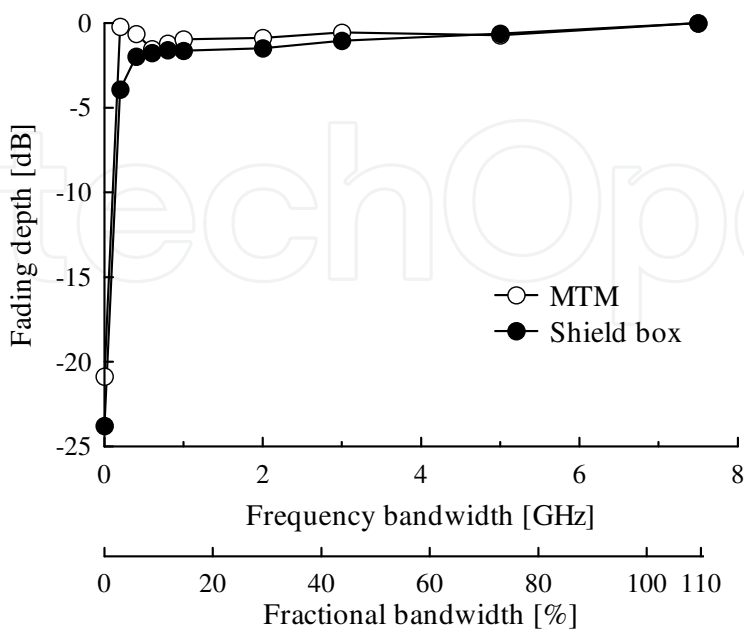


Fig. 7. Fading depth versus occupied bandwidth.

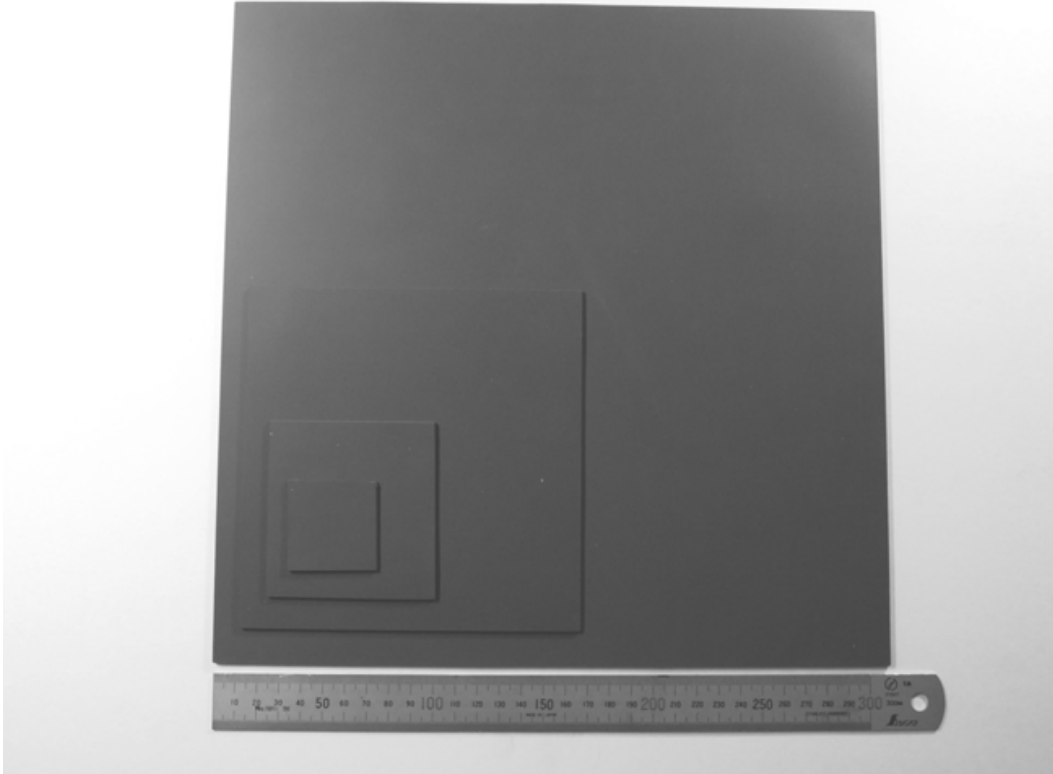


Fig. 8. Examples of radio absorber used in the experiment. The areas are 0.093, 0.023, 0.006, and 0.001 m².

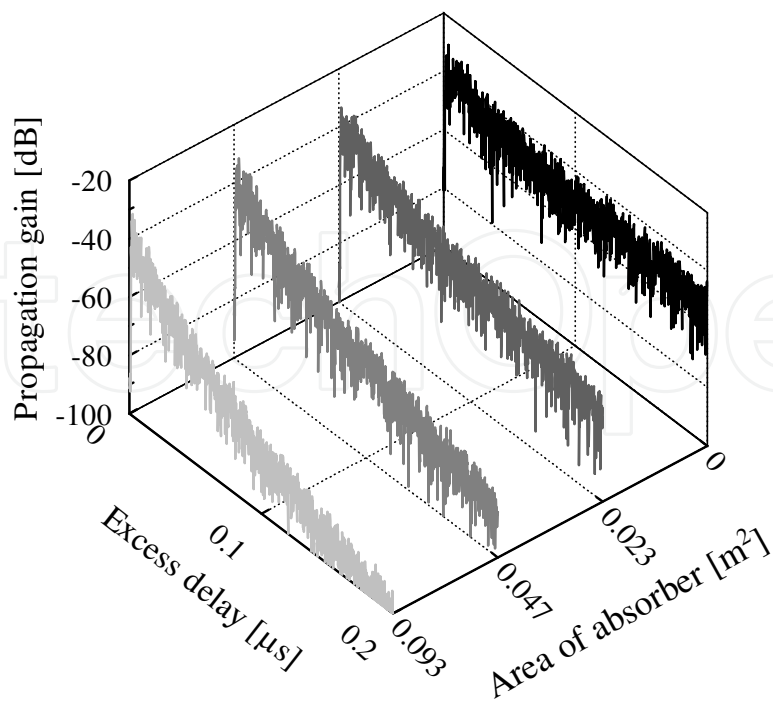


Fig. 9. Delay profiles at (300, 0) in the shield box, for various areas of radio absorber strip.

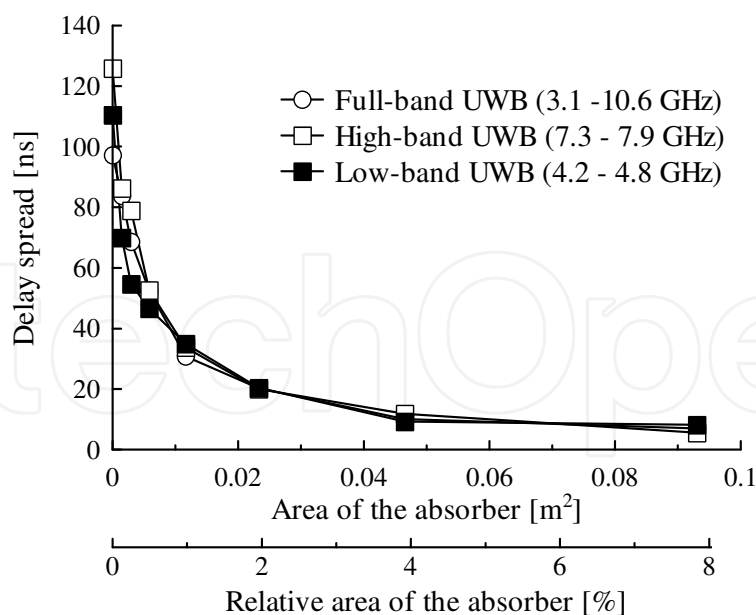


Fig. 10. Delay spread versus area of the absorber at (300, 0).

between the delay spread and the area of radio absorber is depicted in Fig. 10, where the percent area represents the ratio of the area of the radio absorber to the total inner surface area. The relatively small area of the radio absorber successfully suppressed the delay spreads in the shield box: 0.5 and 4% area of the absorber yielded 50 and 10% suppression, respectively. The spatial distributions of delay spread are shown in Fig. 11 with use of the radio absorber covering 8% of the total inner surface. Delay spread ranged from 3.7 to 9.2 ns for full UWB, from 2.3 to 16 ns for the low-band UWB, and from 2.4 to 11 ns for the high-band UWB. Cumulative distribution function (CDF) of delay spread is shown in Fig. 12, which reveals that the median (CDF = 0.5) of the delay spreads were 5.8, 6.9, 6.2 ns for the full-band, the low-band, and the high-band UWB, respectively. The smaller delay spread in the high-band UWB than the low-band UWB were attributable to higher propagation losses in the high-band than in the low-band. Received energy losses caused by the radio absorber were estimated as shown in Fig. 13: 0.5 and 4% area resulted in 2 and 5 dB in energy loss, respectively. The spatial distributions of propagation gain are shown in Fig. 14 with use of the radio absorber covering 8% of the total inner surface. Propagation gain ranged from -24 to -19 dB for full UWB, from -25 to -15 dB for the low-band UWB, and from -29 to -19 dB for the high-band UWB. The gain decreased and fluctuation of the gain increased as the area of the radio absorber increased. Including these energy losses, the relation between the fading depth and the occupied bandwidth was derived. No substantial change in the fading depth was observed as an effect of the radio absorber.

In orthogonal frequency division multiplexing (OFDM), the input data are divided into blocks of the same size, where each block is referred to as an OFDM symbol. By appending a cyclic prefix to each OFDM symbol, the ISI can be removed as long as the cyclic prefix is longer than the impulse response of the channel (typically represented by the delay spread). WiMedia (Heidari, 2008), a high-speed wireless personal area communication standard, utilized multiband OFDM, one of the UWB technologies. It employs 60.61-ns zero postfix (or zero-padded suffix as an alternative to the cyclic prefix). When the delay spreads are suppressed sufficiently shorter than the 60.61 ns, therefore, we can use the WiMedia devices, which yield the maximum data rate of 480 Mb/s, within spacecrafts.

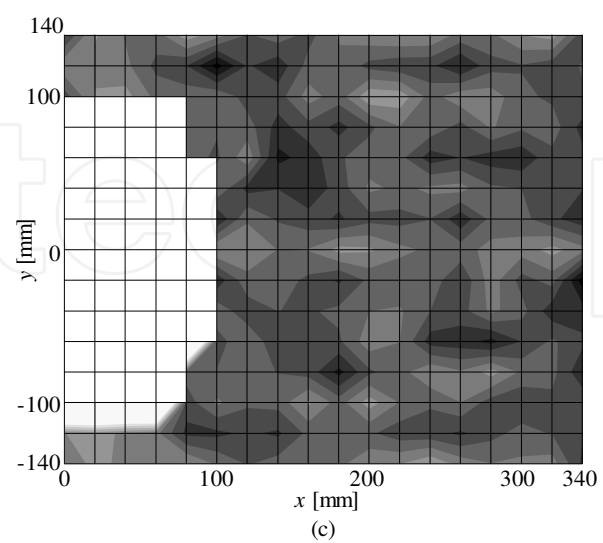
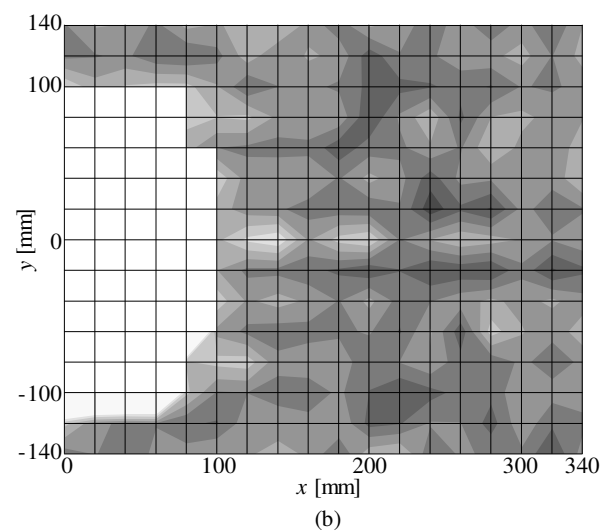
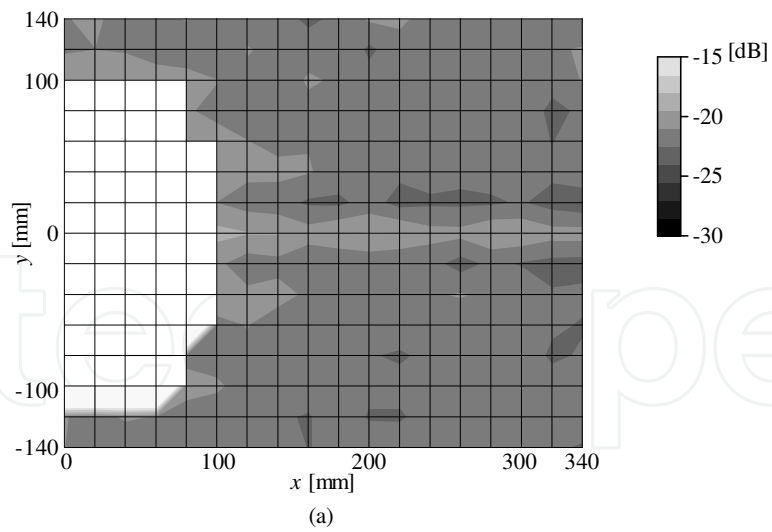


Fig. 11. Spatial distribution of delay spread with use of 0.093 m^2 area of the radio absorber, computed from: (a) full UWB (3.1 - 10.6 GHz), (b) low-band UWB (4.2 - 4.8 GHz), and (c) high-band UWB (7.3 - 7.9 GHz).

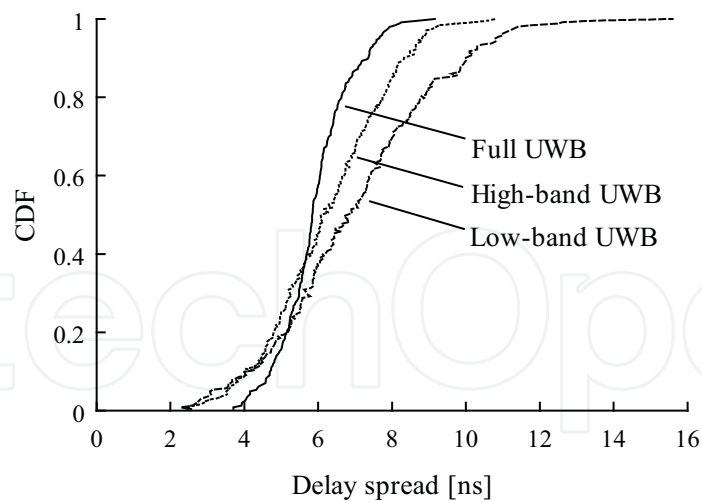


Fig. 12. Cumulative distribution function of delay spread.

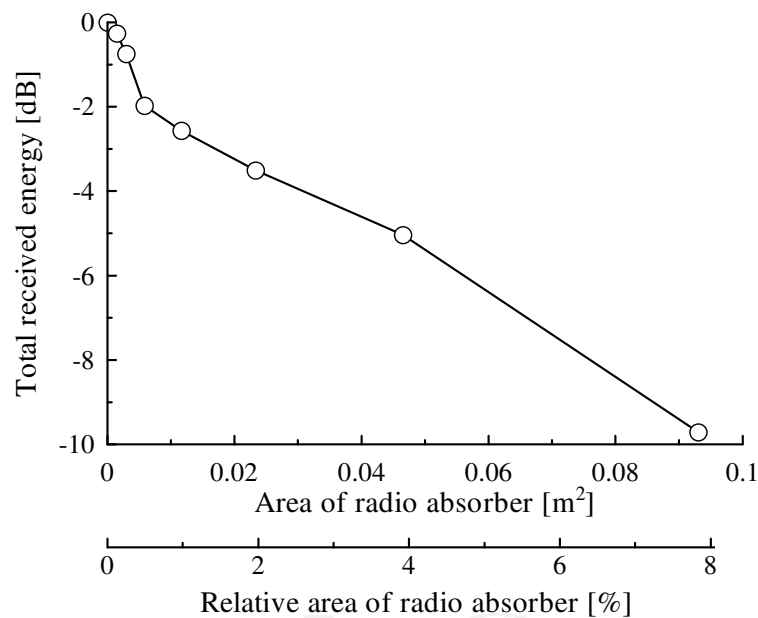


Fig. 13. Received energy loss caused by the radio absorber.

5. Conclusions

Ultra wideband (from 3.1 to 10.6 GHz, from 4.2 to 4.8 GHz, and from 7.3 to 7.9 GHz) and CW (6.85 GHz) propagation were measured and characterized inside a small spacecraft. Major findings are summarized as follows:

- While CW resulted in nearly 30-dB fading at several “dead spots” caused by multipath, UWB yielded no dead spots. The UWB systems have therefore an advantage over narrowband systems from the viewpoint of reducing fading margins.
- A bandwidth over 400 MHz or a fractional bandwidth over 6% was capable of reducing the fading depth by approximately 2 dB in conductive closed spaces like spacecraft.
- The conductive enclosures caused abundant multipaths and, as a result, long delay spreads, particularly when empty.

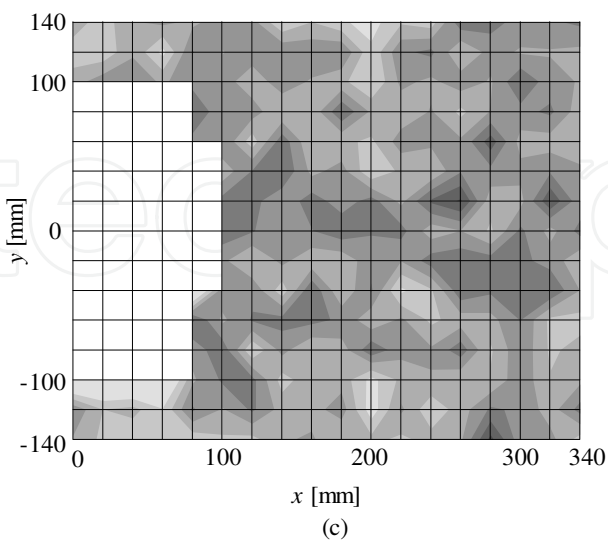
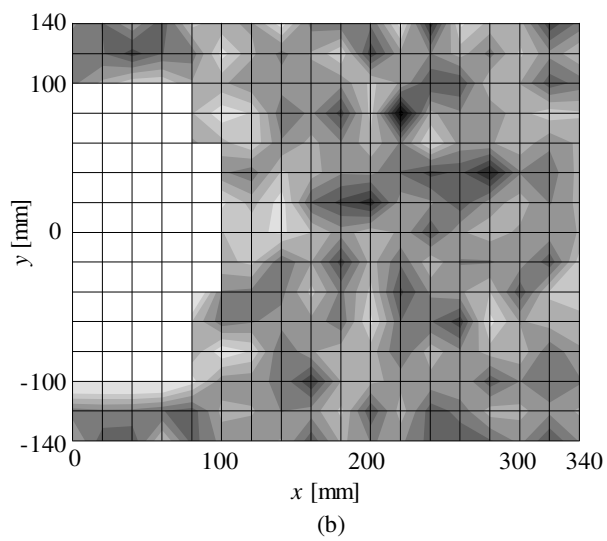
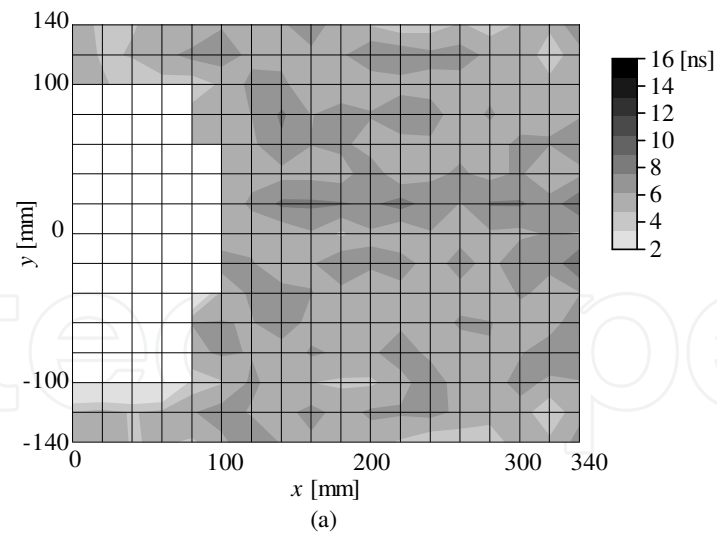


Fig. 14. Spatial distribution of propagation gain with use of 0.093 m^2 area of the radio absorber, measured from: (a) full UWB (3.1 - 10.6 GHz), (b) low-band UWB (4.2 - 4.8 GHz), and (c) high-band UWB (7.3 - 7.9 GHz).

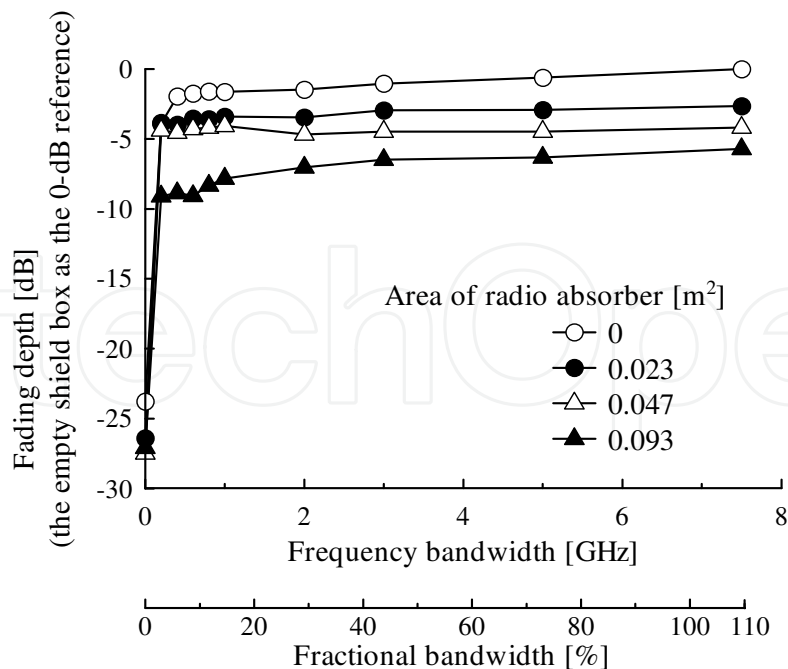


Fig. 15. Fading depth versus occupied bandwidth in the shield box with use of a radio absorber.

- Propagation gain decreased and the fluctuation range of the gain increased when increasing the area of radio absorber.
- The delay spreads can be suppressed with the use of a small patch of radio absorber. For empty enclosures, an 8% area of radio absorber can suppress the delay spreads less than 16 ns (typically 10 ns).
- Commercial, off-the-shelf WiMedia devices can be used to accommodate up to 480-Mb/s data buses within spacecraft, as long as the delay spread is suppressed far below 60 ns, from the viewpoint of propagation.

Future study and concerns include propagation measurements and characterization within larger spacecrafts and electromagnetic compatibility with the other subsystems to realize UWB wireless connection (at least partially) as a replacement for wired data buses.

6. Acknowledgment

This work has been supported in part by the Research Institute for Science and Technology, Tokyo Denki University, under the grant Q10J-07.

7. References

- T. Kobayashi. (2006). Measurements and characterization of ultra wideband propagation channels in a passenger-car compartment. *IEICE Trans. Fundamentals*, vol. E89-A, no. 11 (Nov. 2006), pp. 3089-3094.
- M. Ghavami.; L. B. Michael. & R. Kohn. (2007). *Ultra Wideband Signals and Systems in Communication Engineering*. NY: Wiley, 2nd ed. New York.

- M. Z. Win. & A. Scholtz. (2002). Characterization of ultra-wide bandwidth wireless indoor channels: a communication-theoretic view. *IEEE J. Select. Areas Commun.*, vol. 20, no. 9 (Dec. 2002), pp. 1613-1627.
- J. Foerster. (2002). Channel modelling sub-committee report final. IEEE P802.15-02/368r5-SG3a.
- K. Haneda.; J. Takada. & T. Kobayashi. (2006). Cluster properties investigated from a series of ultrawideband double directional propagation measurements in home environments. *IEEE Trans. Antennas Propag.*, vol. 54, no. 12 (Dec. 2006), pp. 3778-3788.
- Y. Suzuki. & T. Kobayashi. (2005). Ultra wideband signal propagation in desktop environments. *IEICE Trans. Fundamentals*, vol. E88-A, no. 9 (Sep. 2005), pp. 2272-2278.
- J. Gelabelt.; A. Kavatjikidis.; D. J. Edwards. & C. J. Stevens. (2009) Experimental UWB channel characterisation of an electromagnetically small environment, *Proceedings of 2009 Loughborough Antennas and Propagat. Conf. (LAPC 2009)*, Loughborough, UK, Nov. 2009.
- European Cooperation for Space Standardization (2003). Standard ECSS-E-50-12A, SpaceWire – links, nodes, routers and networks.
- T. Taniguchi.; A. Maeda. & T. Kobayashi. (2006). Development of an omnidirectional and low-VSWR ultra wideband antenna. *International Journal on Wireless and Optical Communications*, vol. 3, no. 2 (Aug. 2006), pp. 145-157.
- G. Heidari. (2008). *WiMedia UWB – Technology of Choice for Wireless USB and Bluetooth*. John Wiley & Sons, New York.

IntechOpen



Advances in Spacecraft Technologies

Edited by Dr Jason Hall

ISBN 978-953-307-551-8

Hard cover, 596 pages

Publisher InTech

Published online 14, February, 2011

Published in print edition February, 2011

The development and launch of the first artificial satellite Sputnik more than five decades ago propelled both the scientific and engineering communities to new heights as they worked together to develop novel solutions to the challenges of spacecraft system design. This symbiotic relationship has brought significant technological advances that have enabled the design of systems that can withstand the rigors of space while providing valuable space-based services. With its 26 chapters divided into three sections, this book brings together critical contributions from renowned international researchers to provide an outstanding survey of recent advances in spacecraft technologies. The first section includes nine chapters that focus on innovative hardware technologies while the next section is comprised of seven chapters that center on cutting-edge state estimation techniques. The final section contains eleven chapters that present a series of novel control methods for spacecraft orbit and attitude control.

How to reference

In order to correctly reference this scholarly work, feel free to copy and paste the following:

Akihisa Matsubara, Atsushi Tomiki, Tomoaki Toda and Takehiko Kobayashi (2011). Measurements and Characterization of Ultra Wideband Propagation within Spacecrafts--Proposal of Wireless Transmission for Replacing Wired Interface Buses, *Advances in Spacecraft Technologies*, Dr Jason Hall (Ed.), ISBN: 978-953-307-551-8, InTech, Available from: <http://www.intechopen.com/books/advances-in-spacecraft-technologies/measurements-and-characterization-of-ultra-wideband-propagation-within-spacecrafts-proposal-of-wirel>

INTECH
open science | open minds

InTech Europe

University Campus STeP Ri
Slavka Krautzeka 83/A
51000 Rijeka, Croatia
Phone: +385 (51) 770 447
Fax: +385 (51) 686 166
www.intechopen.com

InTech China

Unit 405, Office Block, Hotel Equatorial Shanghai
No.65, Yan An Road (West), Shanghai, 200040, China
中国上海市延安西路65号上海国际贵都大饭店办公楼405单元
Phone: +86-21-62489820
Fax: +86-21-62489821

© 2011 The Author(s). Licensee IntechOpen. This chapter is distributed under the terms of the [Creative Commons Attribution-NonCommercial-ShareAlike-3.0 License](https://creativecommons.org/licenses/by-nc-sa/3.0/), which permits use, distribution and reproduction for non-commercial purposes, provided the original is properly cited and derivative works building on this content are distributed under the same license.

IntechOpen

IntechOpen